PROCEEDINGS OF SCIENCE

Sterile Neutrino Dark Matter Searches with the KATRIN Experiment

Frank Edzards (for the KATRIN collaboration)[a,b,*]

[a] *Technical University of Munich, TUM School of Natural Sciences, Physics Department, James-Franck-Str. 1, 85748 Garching, Germany*

[b] *Max Planck Institute for Physics, Boltzmannstr. 8, 85748 Garching, Germany*

E-mail: frank.edzards@tum.de

Sterile neutrinos are a natural extension of the Standard Model of particle physics. If their mass is in the keV range, they are a viable dark matter candidate. One way to search for sterile neutrinos in a laboratory-based experiment is via tritium β-decay. A sterile neutrino with a mass of up to 18.6 keV would manifest itself in the electron energy spectrum as a spectral distortion with a kink-like feature. The objective of the TRISTAN project is to extend the KATRIN experiment with a novel multi-pixel silicon drift detector and readout system to search for a keV-scale sterile neutrino signal. This manuscript gives an overview on the current status of the project with an emphasis on the detector performance.

6th International Conference on Technology and Instrumentation in Particle Physics (TIPP2023)
4 - 8 Sep 2023
Cape Town, Western Cape, South Africa

*Speaker

PoS(TIPP2023)102

1. Introduction

Sterile neutrinos are hypothetical, neutral leptons which, unlike the active neutrinos, do not interact weakly. They are a natural extension of the Standard Model of particle physics [1]. If their mass is in the keV range, they are a suitable dark matter candidate [1–4]. Depending on their actual production mechanism, sterile neutrinos could act as warm dark matter. This can help to mitigate tensions between pure cold dark matter scenarios and the observation of small scale structures in our universe [5]. Indirect searches and cosmological observations set stringent limits on the active-sterile neutrino mixing amplitude of $10^{-10} < \sin^2\theta < 10^{-6}$ in a sterile neutrino mass range of $1\,\mathrm{keV} < m_4 < 50\,\mathrm{keV}$ [6–10]. However, these limits are model-dependent and there are several theoretical models that can be deployed to relax the stringent bounds by several orders of magnitude [11].

One method to search for sterile neutrinos in a laboratory-based experiment is via their production in single β-decay. The electron antineutrino (flavor eigenstate) emitted in the decay is a superposition of the neutrino mass eigenstates, including the keV-scale sterile neutrino. As a result, the measured electron energy spectrum is a superposition of the active and sterile neutrino decay branches, see **Fig. 1**. The imprint of the sterile neutrino in the spectrum is a spectral distortion including a kink-like signature which is most prominent at electron energies $E_0 - m_4$, where E_0 denotes the spectral endpoint.

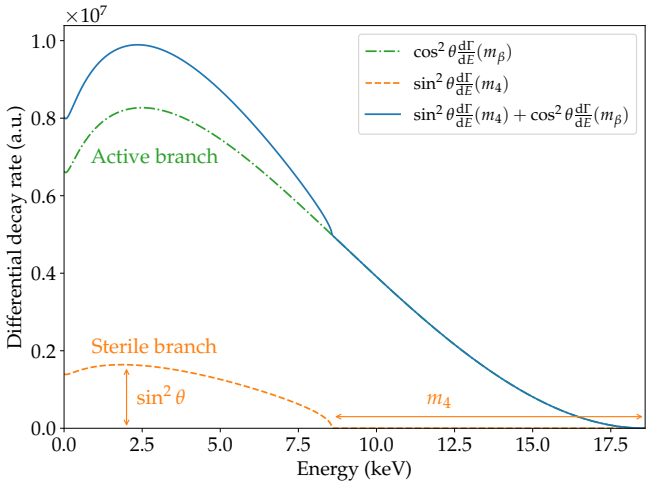

Figure 1: Imprint of a keV-scale sterile neutrino in single β-decay (here using the example of tritium). The measured energy spectrum (blue curve) is a superposition of the decay branches corresponding to the active (green dash-dotted curve) and the sterile neutrino (orange dashed curve), respectively. The amplitude of the sterile branch is given by the mixing amplitude $\sin^2\theta$, whereas the maximal energy is determined by the mass m_4. For illustrative purposes, an unusually large mixing amplitude of $\sin^2\theta \approx 0.2$ has been used.

The Karlsruhe Tritium Neutrino (KATRIN) experiment is well suited to search for keV-scale sterile neutrinos due to its ultra-luminous tritium source. Currently, the experiment measures the effective electron antineutrino mass by investigating the tritium β-decay spectrum in the last 40 eV below the spectral endpoint at $E_0 = 18.6\,\mathrm{keV}$. A final sensitivity of better than $0.3\,\mathrm{eV}/c^2$ (90% C.L.) is

targeted after a total measurement time of 1000 days [12, 13]. Recently, the first sub-eV limit on m_ν of 0.8 eV (90% CL) based on the first two high-activity tritium measurement campaigns has been published [14–16]. The neutrino mass program of KATRIN is foreseen to continue until the end of 2025. Afterwards, the beamline will be upgraded to enable a search for keV-scale sterile neutrinos.

Since the mass associated with a possible sterile neutrino is unconstrained, the spectral distortion and kink-like signature could be located several keV away from the endpoint. In the currently ongoing neutrino mass measurements, only the region around the endpoint is probed. For the keV sterile neutrino search, however, the entire tritium β-decay spectrum will be measured. Therefore, the electron count rate is increased up to levels of 10^8 counts per second (cps). However, the current detector system is limited to a total rate of 10^5 cps integrated over all 148 pixels. To handle the high rate and maintain excellent spectroscopic properties, i.e. an energy resolution of 300 eV full width at half maximum (FWHM) at 20 keV, a multi-pixel silicon drift detector (SDD) and readout system, the TRISTAN detector, is currently being developed. The ultimate goal is to enable the KATRIN experiment to reach a sensitivity to the active-to-sterile mixing amplitude at the parts-per-million (ppm) level. With this, current laboratory limits could be improved by several orders of magnitude and the parameter space of cosmological interest could possibly be reached [17].

2. TRISTAN Detector System

The TRISTAN detector system follows the general design idea of SDDs originally developed for X-ray spectroscopy [18]. The detectors are produced by the Semiconductor Laboratory of the Max Planck Society (HLL). SDDs are semiconductor detectors that use the principle of sideward depletion, see **Fig. 2** [18, 19]. A volume of a high-resistivity semiconductor material, n-type silicon (4 kΩ cm), is covered by rectifying p-doped junctions on both surfaces. The detector bulk is depleted by applying a negative bias voltage on the entrance window side (p+ back contact). Several strip-like segmented p-junctions on the opposite side (readout side) are used as drift rings. These rings are biased such that they generate an electric field with a strong component parallel to the surface towards the anode.

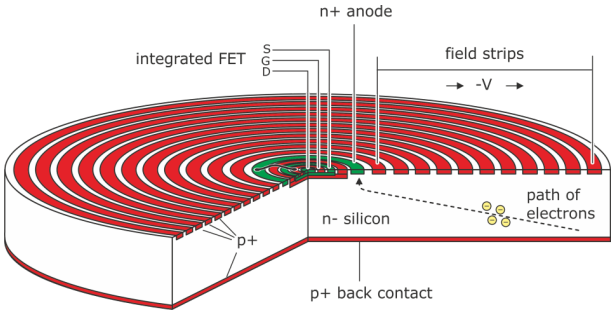

Figure 2: Schematic of a silicon drift detector (single pixel): Electrons are guided by an electric field to the collecting n+ anode in the center of the cell, which is surrounded by several drift rings (p-junctions). The entrance window for radiation is on the opposite side (p+ back contact). The detector features an integrated field-effect transistor (FET) close to the anode which acts as a first amplification stage in the signal readout chain. The dashed line indicates the drift path of electrons to the anode. Figure first published in [19].

As soon as ionizing radiation enters the detector, electron hole pairs are created. The electrons are collected at a small anode (diameter of 82 µm) on the readout side. Due to the small physical dimensions of the electrode, the detector has a small capacitance which is almost independent of the detector area. This allows for low electronic noise and high-rate operation of the SDD. The ultimate noise performance is achieved by integrating a junction field-effect transistor (JFET) into the detector chip near the anode of each pixel. This allows the readout electronics to be placed at several cm distance to the detector chip, while keeping the total anode capacitance at only $O(100\,\mathrm{fF})$ [17, 20]. This is necessary since the final detector system will consist of many pixels arranged in a focal plane array.

The TRISTAN detector is based on many SDD pixels combining a large sensitive area with the energy resolution and the count rate capability of a single SDD. To avoid insensitive detection areas between the cells, hexagonal pixels arranged in a honeycomb pattern are used. In order to minimize detector-related effects such as charge sharing, backscattering, and back-reflection, a pixel size with a circumscribed diameter of 3.3 mm has been chosen [17, 20]. The detector system will be segmented into smaller detector modules, each consisting of 166 pixels with a chip size of $38\times40\,\mathrm{mm}^2$. **Fig. 3** shows a photograph of a single detector module. For the sterile neutrino search with the KATRIN experiment, several detector modules will be mounted next to each other. In the baseline design, the detector system will be composed of nine detector modules with about 1500 pixels.

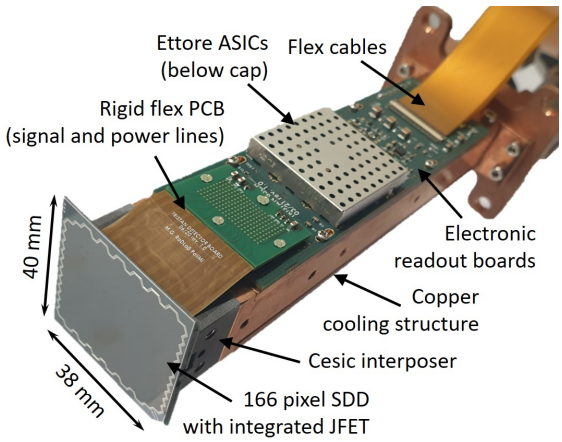

Figure 3: Photograph showing a single TRISTAN detector module. It consists of a monolithic 166-pixel SDD chip which is glued on an interposer made of a silicon ceramic composite called Cesic. The interposer acts as a thermal link to the copper cooling structure. The signal readout electronics are placed in a plane perpendicular to the SDD chip, on two identical electronics readout boards. The boards are mounted on the top and bottom surfaces of the copper cooling structure. Source: [20].

3. Detector Performance

3.1 Performance with X-rays

The spectroscopic performance of the TRISTAN detector system with X-rays has first been investigated with a 7-pixel prototype detector. In measurements with an ^{55}Fe calibration source and a

temperature of −30°C at the SDD chip, an energy resolution of less than 140 eV FWHM at the 5.9 keV peak (Mn-Kα line) was measured. Moreover, using an ^{241}Am calibration source, it was shown that the detector features an excellent linearity of 0.1% in the energy range 10 − 60 keV [21]. For the 166-pixel detector module, a similar performance was achieved: An average energy resolution of about 144 eV FWHM at the Mn-Kα line was obtained [20]. The energy resolution at the Mn-Kα line of all pixels is shown in the pixel map in **Fig. 4**. They show a very homogeneous performance in terms of energy resolution. Just as for the 7-pixel detector, the linearity of the energy scale has been investigated using an ^{241}Am calibration source. A linearity of 0.5% in the energy range 10 − 60 keV was obtained. Finally, dedicated long-term measurements revealed that the detector system features an excellent spectroscopic stability with variations on the sub-percent level over a period of 63 h [20].

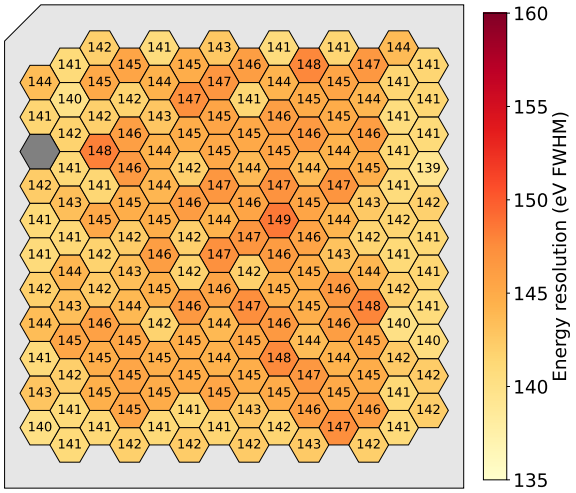

Figure 4: Pixel map showing the energy resolution of all cells at the 5.9 keV Mn-Kα line measured using an ^{55}Fe calibration source. The values within the pixels denote the energy resolution in units of eV FWHM. The average energy resolution of all pixels is 143.7 eV FWHM (energy filter rise time of 2 µs). The pixel in grey had to be disabled due to connection problems. Source: [20].

3.2 Performance with Electrons

One of the main challenges of using the TRISTAN detector system for a keV sterile neutrino search arises from the application of the SDD technology to electron spectroscopy. In the KATRIN experiment, the electrons will hit the detector with a maximum energy of 38.6 keV, which is the sum of the spectral endpoint E_0 = 18.6 keV, and an optional accelerating potential of up to 20 kV. As soon as the electrons hit the entrance window, they deposit their kinetic energy in the detector volume by scattering along a path of several µm [25]. As opposed to the detection of X-rays, several detector-related effects have to be taken into account when SDDs are used for electron detection. The main effects to be considered are 1) an incomplete charge collection at the detector entrance window, 2) charge sharing between pixels, and 3) detector backscattering. A typical energy spectrum for monoenergetic electrons is shown in **Fig. 5**. The spectrum not only shows the main peak, but also a low-energy tail close to that peak, and a pronounced tail towards smaller energies.

When modeling the detector response for the keV sterile neutrino search, all these effects must be well understood and have to be taken into account.

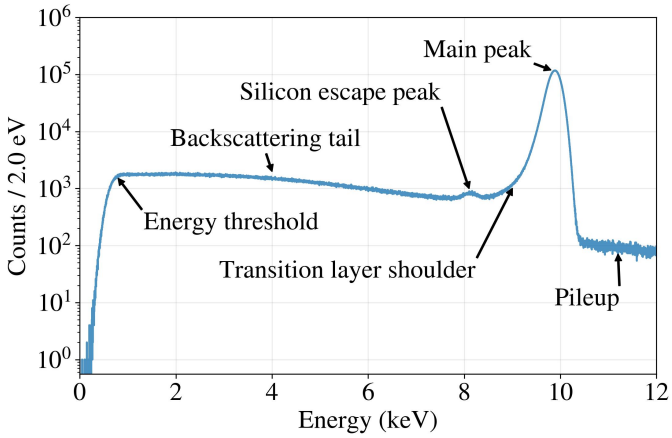

Figure 5: Energy spectrum showing a measurement of monoenergetic electrons of 10 keV with a 7-pixel prototype detector. The response is characterized by different features such as charge sharing between neighboring pixels, detector backscattering, and readout electronics effects. Source: [30].

Charge collection at the entrance window The first effect to be considered is due to an incomplete charge collection at the entrance window of the detector. The entrance window surface is covered by a 10 nm-thick silicon dioxide (SiO_2) layer. As SiO_2 acts as an insulator, the electric field in this region is so weak that only high-energetic secondary electrons can reach the sensitive volume. Consequently, most of the charges are not collected and the charge collection efficiency (CCE) is close to zero. A second contribution to the incomplete charge collection at the entrance window can be related to the doping profile. As it reaches several tens of nanometers in the bulk, the CCE gradually increases to 100%, see **Fig. 6** [26]. This entrance window region with zero and increasing CCE is commonly referred to as dead layer.

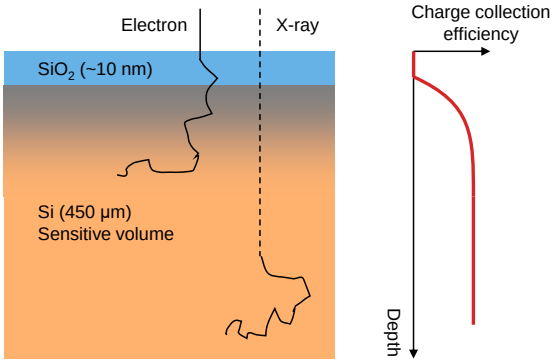

Figure 6: Charge collection efficiency (CCE) at the entrance window of an SDD. While the CCE of X-rays is hardly affected (due to rather higher penetration depths), electrons directly start scattering when hitting the entrance window surface of the detector. In the 10 nm-thick SiO_2 layer, their CCE is close to zero (plot on the right-hand side). In the layer below, the CCE increases gradually. Figure courtesy of K. Urban.

Since X-rays have comparably high penetration depths in silicon, their detection is typically hardly affected by the effects described above. As opposed to this, electrons have an energy deposition profile with a pronounced component in close proximity to the entrance window. As a result, a fraction of their energy is lost in this region. This gives rise to a shift of the main electron peak towards lower energies. Moreover, the full energy peak becomes asymmetric featuring a pronounced low-energy tail. This effectively worsens the energy resolution of the detection system. For the 7-pixel prototype detectors, an energy shift of about 30 eV has been measured for electrons with an energy of 30.4 keV (using a ^{83m}Kr calibration source). Moreover, assuming a simplified step-like dead layer model, an entrance window thickness of < 50 nm could be determined [22]. It should be noted here that this value is a rough estimation; a more realistic model can be found in [23, 24]. The impact of the dead layer on the electron energy spectrum is illustrated in **Fig. 7**.

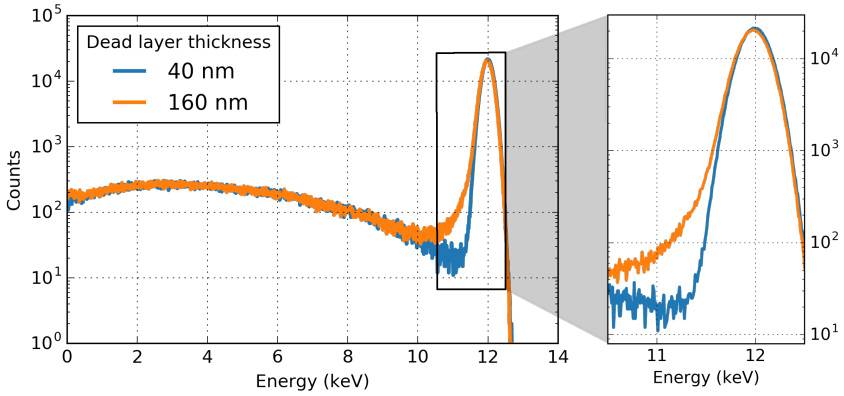

Figure 7: Simulation showing the impact of the dead layer thickness on the electron response. For higher thicknesses, a pronounced low-energy tail can be observed. Furthermore, the main electron peak is slightly shifted to smaller energies. Source: [26].

Charge sharing The effect of charge sharing appears when an electron hits the detector at or close to the boundary of neighboring pixels. Due to the spatial extension of the generated charge cloud, the charge carriers are separated at the pixel boundary and drift to the anodes of the respective cells. This results in measurable signals in all pixels involved with a summed energy, which is equal to the deposited energy of the incident radiation. Charge sharing can occur between two or three adjacent pixels[1]. It is characterized by the size of the charge cloud and is of major importance for modeling the detector response [26–28].

Dedicated measurements with a 7-pixel prototype detector as well as simulations were carried out to characterize the effect of charge sharing. The experimental setup consists of a pulsed laser, whose beam is directed onto the entrance window of the detector using fiber optics. The laser has been chosen such that its photon beam mimics an electron signal in the detector. More details on the setup can be found in [27, 28]. A grid scan in the area where three pixels are adjacent to each other (triple point) was performed. An empirical model was developed to describe the signal

[1] In principle, charge sharing can even occur between more than three pixels. This is possible when backscattered electrons are reflected back onto the detector surface via the magnetic fields in the KATRIN detector section.

shape and extract relevant parameters such as the amplitude of the signals. **Fig. 8a** shows the reconstructed energy distribution at the boundary of three adjacent pixels. It can be observed how the reconstructed energy is divided between the pixels. The sum of the energies deposited in the different pixels yields the total deposited energy. The reconstructed energy along a slice of two adjacent cells is shown in **Fig. 8b**. This energy distribution was modeled with a Gaussian distribution with width w describing the effective width of the charge cloud. A value of $w \leq (16.3 \pm 0.2)\,\mu\text{m}$ was measured which is in very good agreement with the value obtained in field and pulse shape simulations [28].

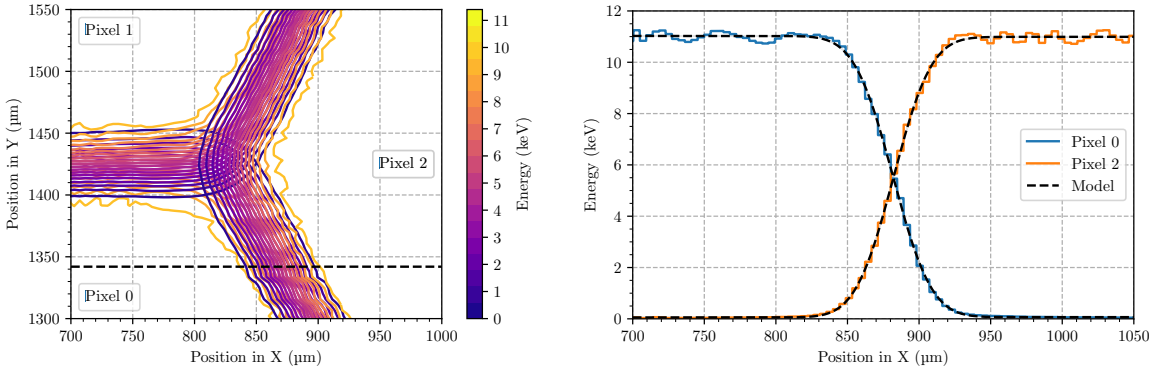

(a) Energy distribution at the triple point.

(b) Reconstructed energy at pixel boundary.

Figure 8: Charge sharing measurements with a 7-pixel detector and a pulsed laser (beam energy of roughly 11 keV). (a) Energy distribution at the boundary of three adjacent pixels (triple point). The contour lines enclose areas of the pixels in which the same amount of charge was collected. (b) Reconstructed energy as a function of the position along the dashed line indicated in (a). Source: [27].

Backscattering Another effect of incomplete charge collection in an SDD can be related to the backscattering of electrons. The incoming electrons as well as secondary electrons produced in the detector volume undergo scattering. As a result, the electrons can change their directions of movement such that they eventually leave the active volume before having deposited their entire energy. In the energy spectrum, this gives rise to an extended continuum towards lower energies, the so-called backscattering tail, see **Fig. 5**. The amount of backscattering depends on the initial energy E_I and incident angle Θ_I of the incoming electron[2]. Lower electron energies and higher incident angles result in a smaller penetration depth and thus increase the likelihood of an electron escape [20, 29, 30].

To characterize the effect of detector backscattering, dedicated measurements with a tandem SDD system and a custom-designed electron source were performed. A 7-pixel detector served as an active target, whereas a 166-pixel detector was used to measure the backscattered electrons. Monoenergetic electrons were produced using a custom electron gun based on the effect of thermionic emission. It consists of a thin electrically heated tantalum filament on a high electrical potential, which accelerates the electrons and provides rates of more than 100 kcps [25]. In the measurements, monoenergetic electrons with different energies (5, 7.5, 10 keV) and incident angles (0°, 31°, 59°)

[2]The incident angle of an electron beam perpendicular to the detector surface is 0°.

were directed onto the 7-pixel detector. **Fig. 9** shows the backscattering coefficient[3] η as a function of the incident angle Θ_I for the different energies E_I. It can be observed that the backscattering increases with increasing incident angle. In addition, a slight decrease of the coefficient is observed with increasing electron energy. The measurement results agree very well with dedicated GEANT4 simulations. More details of the backscattering investigations are discussed in [29, 30].

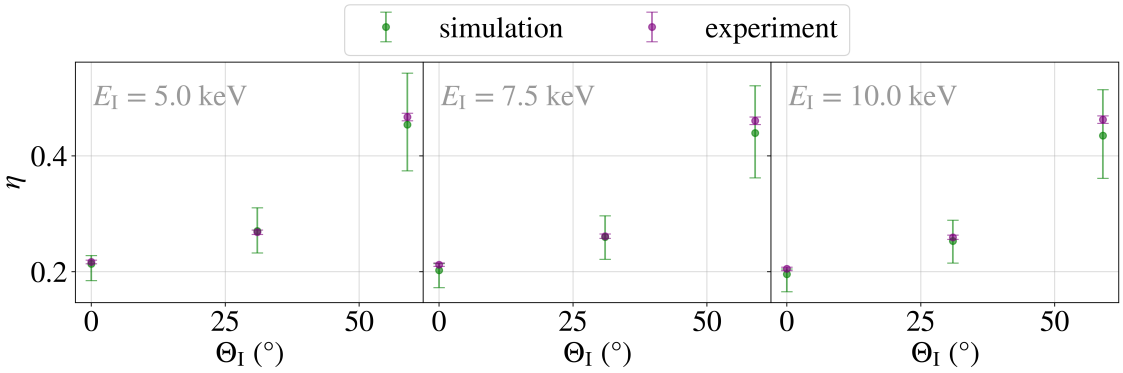

Figure 9: Backscattering coefficient η as a function of the incident angle Θ_I for different initial electron energies E_I. The detector backscattering strongly increases with incident angle and slightly decreases with energy. Source: [30].

4. KATRIN in the Sterile Neutrino Landscape

The goal of the TRISTAN project is to search for keV-scale sterile neutrinos with the KATRIN experiment in the entire phase space of tritium β-decay. A sensitivity on the mixing amplitude of $\sin^2\theta < 10^{-6}$ is targeted. The sensitivity projection in the global landscape (including other relevant searches) is shown in **Fig. 10**.

In the currently ongoing neutrino mass measurements, the KATRIN experiment can already probe the parameter space for light sterile neutrinos in the eV mass range. These sterile neutrinos are motivated by anomalies in short-baseline neutrino oscillation experiments [31–35]. Based on the first two measurement campaigns [36, 37], the KATRIN experiment could already exclude a large region of the phase space of the gallium anomaly as observed by the GALLEX, SAGE, and BEST experiments [33–35]. Moreover, during the first commissioning run of the KATRIN experiment, a measurement with a reduced source activity and an extended measurement interval for sterile neutrinos with masses of up to 1.6 keV was performed. A mixing amplitude of $\sin^2\theta < 5 \cdot 10^{-4}$ for a sterile neutrino mass of $m_4 = 300$ eV could be excluded. The result improves existing laboratory bounds in the sterile neutrino mass range $0.1 < m_4 < 1.0$ keV [38].

In the scope of the TRISTAN project, the KATRIN collaboration plans to extend the measurement range to the entire energy spectrum of tritium β-decay. Thus, existing laboratory limits to keV-scale

[3]The backscattering coefficient is the ratio of electrons detected in the backscattering detector to those measured in the target detector. It is scaled by the detection efficiency obtained from simulations [30].

sterile neutrinos, see references [39–44], can be improved by several orders of magnitude [21]. The keV sterile neutrino searches of the KATRIN collaboration are highly complementary to the measurement efforts of other collaborations, i.e. BeEST [45] and HUNTER [46]. These collaborations search for sterile neutrinos in the high keV mass range using the electron capture reactions of ^{7}Be and ^{131}Cs, respectively. They have the highest sensitivity at several tens to hundreds of keV.

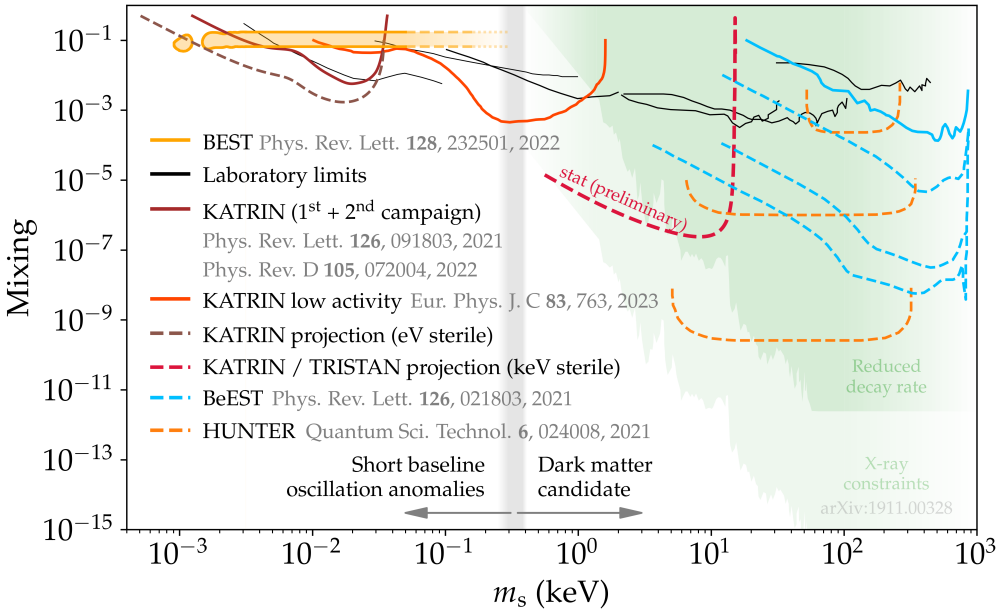

Figure 10: Exclusion contours (solid lines) and sensitivity projections (dashed lines) of ongoing sterile neutrino searches. While sterile neutrinos on the eV mass scale are motivated by anomalies in short-baseline neutrino oscillation experiments, keV-scale sterile neutrinos are suitable dark matter candidates. Current laboratory limits (thin black lines) are based on references [39–44]. The goal of the TRISTAN project is to improve these limits by several orders of magnitude by performing a keV sterile neutrino search with the KATRIN experiment. The sterile neutrino searches of the KATRIN collaboration are highly complementary to other ongoing measurements efforts, such as the BeEST [45] and HUNTER experiments [46]. Indirect searches and cosmological observations based on deep field X-ray measurements of galactic clusters and galaxies are indicated by the green shaded area. These stringent limits are model-dependent and can be relaxed in several theories [11].

Acknowledgements

We acknowledge the support of Helmholtz Association (HGF), Ministry for Education and Research BMBF (05A23PMA, 05A23PX2, 05A23VK2, and 05A23WO6), the doctoral school KSETA at KIT, Helmholtz Initiative and Networking Fund (grant agreement W2/W3-118), Max Planck Research Group (MaxPlanck@TUM), and Deutsche Forschungsgemeinschaft DFG (GRK 2149 and SFB-1258) in Germany; Ministry of Education, Youth and Sport (CANAM-LM2015056, LTT19005) in the Czech Republic; Istituto Nazionale di Fisica Nucleare (INFN) in Italy; the National Science, Research and Innovation Fund via the Program Management Unit for Human Resources & Institutional Development, Research and Innovation (grant B37G660014) in Thailand;

and the Department of Energy through grants DE-FG02-97ER41020, DE-FG02-94ER40818, DE-SC0004036, DE-FG02-97ER41033, DE-FG02-97ER41041, DE-SC0011091 and DE-SC0019304 and the Federal Prime Agreement DE-AC02-05CH11231 in the United States. This project has received funding from the European Research Council (ERC) under the European Union Horizon 2020 research and innovation programme (grant agreement No. 852845). We thank the computing cluster support at the Institute for Astroparticle Physics at Karlsruhe Institute of Technology, Max Planck Computing and Data Facility (MPCDF), and the National Energy Research Scientific Computing Center (NERSC) at Lawrence Berkeley National Laboratory.

References

[1] R. Adhikari *et al.*: A White Paper on keV sterile neutrino Dark Matter. JCAP 01, 025, 2017. doi:10.1088/1475-7516/2017/01/025

[2] S. Dodelson and L. M. Widrow: Sterile neutrinos as dark matter. Phys. Rev. Lett. 72, 17, 1994. doi:10.1103/PhysRevLett.72.17

[3] X. Shi and G. M. Fuller: New Dark Matter Candidate: Nonthermal Sterile Neutrinos. Phys. Rev. Lett. 82, 2832, 1999. doi:10.1103/PhysRevLett.82.2832

[4] A: Boyarsky *et al.*: Sterile neutrino Dark Matter. Prog. Part. Nucl. Phys. 104, 2019. doi:10.1016/j.ppnp.2018.07.004

[5] R. Murgia *et al.*: "Non-cold" dark matter at small scales: a general approach. JCAP 11, 046, 2017. doi:10.1088/1475-7516/2017/11/046

[6] A. Boyarsky *et al.*: A lower bound on the mass of dark matter particles. JCAP 03, 005, 2009. doi:10.1088/1475-7516/2009/03/005

[7] V. K. Narayanan *et al.*: Constraints on the Mass of Warm Dark Matter Particles and the Shape of the Linear Power Spectrum from the Lyα Forest. ApJ 543, L103, 2000. doi:10.1086/317269

[8] U. Seljak *et al.*: Can Sterile Neutrinos Be the Dark Matter? Phys. Rev. Lett. 97, 191303, 2006. doi:10.1103/PhysRevLett.97.191303

[9] B. W. Lee and R. E. Shrock: Natural suppression of symmetry violation in gauge theories: Muon- and electron-lepton-number nonconservation. Phys. Rev. D 16, 1444, 1977. doi:10.1103/PhysRevD.16.1444

[10] P. B. Pal and L. Wolfenstein: Radiative decays of massive neutrinos. Phys. Rev. D 25, 766, 1982. doi:10.1103/PhysRevD.25.766

[11] C. Benso *et al.*: Prospects for finding sterile neutrino dark matter at KATRIN. Phys. Rev. D 100, 115035, 2019. doi:10.1103/PhysRevD.100.115035

[12] J. Angrik *et al.*: KATRIN design report. FZKA 7090, 2005. doi:10.5445/IR/270060419

[13] M. Aker *et al.*: The design, construction, and commissioning of the KATRIN experiment. JINST 16, T08015, 2021. doi:10.1088/1748-0221/16/08/T08015

[14] M. Aker *et al.*: Improved Upper Limit on the Neutrino Mass from a Direct Kinematic Method by KATRIN. Phys. Rev. Lett. 123, 221802, 2019. doi:10.1103/PhysRevLett.123.221802

[15] M. Aker *et al.*: Analysis methods for the first KATRIN neutrino-mass measurement. Phys. Rev. D 104, 012005, 2021. doi:10.1103/PhysRevD.104.012005

[16] M. Aker *et al.*: Direct neutrino-mass measurement with sub-electronvolt sensitivity. Nat. Phys. 18, 160-166, 2022. doi:10.1038/s41567-021-01463-1

[17] M. Aker *et al.*: KATRIN: status and prospects for the neutrino mass and beyond. J. Phys. G: Nucl. Part. Phys. 49, 100501, 2022. doi:10.1088/1361-6471/ac834e

[18] P. Lechner *et al.*: Silicon drift detectors for high count rate X-ray spectroscopy at room temperature. Nucl. Instrum. Meth. A 458, 281, 2001. doi:10.1016/S0168-9002(00)00872-X

[19] P. Lechner *et al.*: Silicon drift detectors for high resolution room temperature X-ray spectroscopy. Nucl. Instrum. Meth. A 377, 346, 1996. doi:10.1016/0168-9002(96)00210-0

[20] D. Siegmann, F. Edzards *et al.*: Development of a Silicon Drift Detector Array to Search for keV-scale Sterile Neutrinos with the KATRIN Experiment. J. Phys. G: Nucl. Part. Phys. 51, 085202, 2024. doi:10.1088/1361-6471/ad4bf8

[21] S. Mertens *et al.*: A novel detector system for KATRIN to search for keV-scale sterile neutrinos. J. Phys. G: Nucl. Part. Phys. 46, 065203, 2019. doi:10.1088/1361-6471/ab12fe

[22] S. Mertens *et al.*: Characterization of silicon drift detectors with electrons for the TRISTAN project. J. Phys. G: Nucl. Part. Phys. 48, 015008, 2021. doi:10.1088/1361-6471/abc2dc

[23] M. Biassoni *et al.*: Electron spectrometry with Silicon drift detectors: a GEANT4 based method for detector response reconstruction. Eur. Phys. J. Plus 136, 125, 2021. doi:10.1140/epjp/s13360-021-01074-y

[24] A. Nava *et al.*: A Geant4-based model for the TRISTAN detector. J. Phys. Conf. Ser. 2156, 012177. doi:10.1088/1742-6596/2156/1/012177

[25] K. Urban *et al.*: A thermionic electron gun to characterize silicon drift detectors with electrons. JINST 19, P06004, 2024. doi:10.1088/1748-0221/19/06/P06004

[26] T. Brunst: First generation prototype detectors for the TRISTAN project. PhD thesis. Technical University of Munich, 2020. Thesis link

[27] C. Forstner: Characterization of a TRISTAN Silicon Drift Detector Array with a Laser System. Master thesis. Technical University of Munich, 2023. Thesis link

[28] C. Forstner *et al.*: Investigation of Charge Collection and Signal Timing in a TRISTAN Silicon Drift Detector. Publication in preparation, 2024.

[29] D. Spreng: Electron Backscattering on Silicon Drift Detectors and Its Impact on a Sterile Neutrino Search with KATRIN. Master thesis. Technical University of Munich, 2023. Thesis link

[30] D. Spreng *et al.*: Investigation of Electron Backscattering on Silicon Drift Detectors for the Sterile Neutrino Search with KATRIN. Publication in preparation, 2024.

[31] A. Aguilar *et al.*: Evidence for neutrino oscillations from the observation of $\bar{\nu}_e$ appearance in a $\bar{\nu}_\mu$ beam. Phys. Rev. D 64, 112007, 2001. doi:10.1103/PhysRevD.64.112007

[32] A. A. Aguilar-Arevalo *et al.*: Phys. Rev. Lett. 121, 221801, 2018. doi:10.1103/PhysRevLett.121.221801

[33] W. Hampel *et al.*: Final results of the ^{51}Cr neutrino source experiments in GALLEX. Phys. Lett. B, 420, 114, 1998. doi:10.1016/S0370-2693(97)01562-1

[34] J. N. Abdurashitov *et al.*: Measurement of the solar neutrino capture rate with gallium metal. III. Results for the 2002–2007 data-taking period. Phys. Rev. C 80, 015807, 2009. doi:10.1103/PhysRevC.80.015807

[35] V. V. Barinov *et al.*: Results from the Baksan Experiment on Sterile Transitions (BEST). Phys. Rev. Lett. 128, 232501, 2022. doi:10.1103/PhysRevLett.128.232501

[36] M. Aker *et al.*: Bound on 3+1 Active-Sterile Neutrino Mixing from the First Four-Week Science Run of KATRIN. Phys. Rev. Lett. 126, 091803, 2021. doi:10.1103/PhysRevLett.126.091803

[37] M. Aker *et al.*: Improved eV-scale sterile-neutrino constraints from the second KATRIN measurement campaign. Phys. Rev. D 105, 072004, 2022. doi:10.1103/PhysRevD.105.072004

[38] M. Aker *et al.*: Search for keV-scale sterile neutrinos with the first KATRIN data. Eur. Phys. J. C 83:763, 2023. doi:10.1140/epjc/s10052-023-11818-y

[39] A. I. Belesev *et al.*: The search for an additional neutrino mass eigenstate in the 2–100 eV region from 'Troitsk nu-mass' data: a detailed analysis. J. Phys. G: Nucl. Part. Phys. 41, 015001, 2014. doi:10.1088/0954-3899/41/1/015001

[40] M. A. Acero *et al.*: White Paper on Light Sterile Neutrino Searches and Related Phenomenology. Snowmass 2021. doi:10.48550/arXiv.2203.07323

[41] J. N. Abdurashitov *et al.*: First measurements in search for keV sterile neutrino in tritium beta-decay in the Troitsk nu-mass experiment. Jetp Lett. 105, 753, 2017. doi:10.1134/S0021364017120013

[42] E. Holzschuh *et al.*: Search for heavy neutrinos in the β-spectrum of ^{63}Ni. Phys. Lett. B 451, 247, 1999. doi:10.1016/S0370-2693(99)00200-2

[43] E. Holzschuh *et al.*: The β-spectrum of ^{35}S and search for the admixture of heavy neutrinos. Phys. Lett. B 482, 1, 2000. doi:10.1016/S0370-2693(00)00476-7

[44] K. Schreckenback *et al.*: Search for mixing of heavy neutrinos in the β^+ and β^- spectra of the ^{64}Cu Decay. Phys. Lett. B 129, 265, 1983. doi:10.1016/0370-2693(83)90858-4

[45] S. Friedrich *et al.*: Limits on the Existence of sub-MeV Sterile Neutrinos from the Decay of ^{7}Be in Superconducting Quantum Sensors. Phys. Rev. Lett. 126, 021803, 2021. doi:10.1103/PhysRevLett.126.021803

[46] C. J. Martoff *et al.*: HUNTER: precision massive-neutrino search based on a laser cooled atomic source. Quantum Sci. Technol. 6, 024008, 2021. doi:10.1088/2058-9565/abdb9b